Journal of Applied Electrochemistry (2021) 51:1083–1092
https://doi.org/10.1007/s10800-021-01559-9

RESEARCH ARTICLE

Preparation and electrochemical properties of porous carbon materials derived from waste hollow fiber filter membrane

He Zhu[1] · Zhishang Gao[1] · Songhong Fan[1] · Mingjian Zhang[1] · Zhangzhang Tang[1] · Zhong Ren[1] · Huixia Feng[1] · Heming Luo[1] · Jianqiang Zhang[1]

Received: 11 July 2020 / Accepted: 10 March 2021 / Published online: 5 April 2021

Abstract

In this paper, waste hollow fiber filter membrane is used as a carbon source and KOH as an activator under an atmosphere of protective argon gas to prepare hollow fiber filter membrane-based porous carbon material ZKC-T via a high-temperature pyrolysis activation method. Hollow fiber filter membrane-based porous carbon ZKC-T was found to consist of amorphous carbon, with an irregular three-dimensional network interconnecting pore structure, specific surface area of up to 2934 $m^2 g^{-1}$, and a reasonable pore size distribution. Cyclic voltammetry and constant current charge and discharge tests showed that the hollow fiber filter-based porous carbon material ZKC-700 has excellent electrochemical performance. The carbon material shows a specific capacitance of up to 289 F g^{-1} at a current density of 1 A g^{-1} in 6 M KOH electrolyte. In addition, the material shows good cycle stability; after 5000 charge and discharge cycles, the capacitance retention rate is as high as 92.8%. The hollow fiber filter membrane-based porous carbon prepared by this method exhibits excellent electrochemical properties.

Graphic abstract

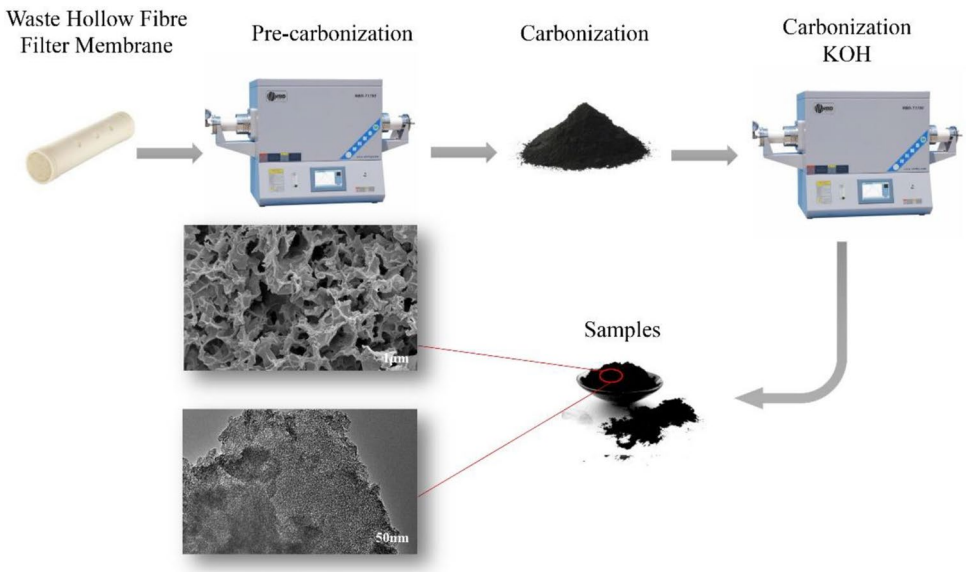

Keywords Waste hollow fiber filter membrane · Porous carbon material · Supercapacitor · Specific surface area · Electrochemical performance

Extended author information available on the last page of the article

1 Introduction

Since the introduction of supercapacitors, research into supercapacitor electrode materials has been prevalent [1–8]. Electrode materials are the core component of supercapacitors. Carbon materials have become one of the most widely used electrode materials in current research based on their low cost, environmental protection, and high efficiency [9–15]. Studies have shown that the specific surface area and pore size distribution of a material are important factors that can affect the performance of carbon materials. Therefore, it is highly important in the research for carbon materials to find a more effective preparation method to regulate the specific surface area and pore size distribution of materials. Jiang et al. used $CaCO_3$ as a template to successfully prepare polytetrafluoroethylene waste into porous carbon through a template carbonization method. For a PTFE:$CaCO_3$:CO $(NH_2)_2$ mass ratio of 2:1:2, the specific surface area was determined to be 1048.2 $m^2\ g^{-1}$, and the specific capacitance of the PTFE composite was found to be 237.8 F g^{-1} at a current density of 1 A g^{-1}. These results show that the carbonization temperature and raw material mass ratio play a crucial role in regulating pore structure [16]. Zhang et al. used waste polystyrene foam as a carbon source and silica particles to create a rich porous structure. A Friedel–Crafts reaction was successfully used to produce a porous carbon material with a 3D network structure. The prepared material showed a specific surface area of 620 $m^2\ g^{-1}$ and a uniform mesopore distribution in the bulk phase. The specific capacitance of the prepared porous carbon material was determined to be 208 F g^{-1} at a current density of 1 A g^{-1} [17].

As we all know, the accumulation of polymer products can lead to environmental pollution and resource waste. Therefore, recycling policies have been adopted to recover polymer waste and reprocess it into useful products. The hollow fiber filter membrane is a common separation membrane, with certain selective permeability, which is widely utilized in the field of water purification. The hollow fiber filter membrane needs to be replaced regularly, and the replaced hollow fiber filter results in polymer waste, which can easily cause harm to the environment. This chapter uses waste hollow fiber filter membrane as a carbon source, which mainly contains polypropylene. Hollow fiber filter membrane-based porous carbon material, ZKC-T, was prepared by a high temperature chemical activation method using argon gas as protective gas and KOH as activator. The crystal structure, microstructure and composition of the fiber ZKC-T was characterized and analysed, and the effects of different carbonization temperatures and activator concentrations on the electrochemical performance of the hollow fiber filter membrane-based porous carbon material were studied. This research can make full use of resources and reduce environmental pollution, and provides an experimental basis for the research and development of solid waste polymer-based porous carbon electrode materials.

2 Experimental

2.1 Preparation of hollow fiber filter membrane-based porous carbon material

2.1.1 Preparation for carbonization

A discarded hollow fiber filter membrane was cut into strips and placed into a porcelain boat. This boat was then placed into a tube furnace, wherein argon gas was passed as a protective gas before raising the temperature to 600° C at a rate of 5 °C/min. The temperature was kept constant at 600° C for 2 h. After natural cooling, the product was collected, and black carbonization powder was obtained by grinding.

2.1.2 Preparation of hollow fiber filter membrane-based porous carbon material

The obtained carbonization and KOH activator were evenly mixed and fully ground, and, then, placed into a tube furnace under an atmosphere of protective argon gas before being heated to a target temperature at a rate of 3 °C/min. The temperature was then maintained at a constant value for 2 h. After cooling to room temperature naturally, the black solid product was stirred and washed with 1 M hydrochloric acid solution, and then the sample was repeatedly washed with ultrapure water until it became neutral and filtered. Finally, after vacuum drying at 80 °C for 12 h, a porous carbon material based on hollow fiber filter membranes was obtained.

2.2 Structural performance characterization

The microstructure and morphology of the porous carbon materials were characterized by transmission electron microscopy (JEM-1200EX, JEOL). The crystal structure was characterized by X-ray diffraction (RINT-2000, Nippon Science). The molecular vibration, rotation, and material properties of the carbon materials were characterized by Raman spectroscopy (JY-HR800, Horiba Scientific Group). X-ray photoelectron spectroscopy (ESCALAB 250Xi, Thermo Fisher Scientific) was used to identify the functional groups and elemental compositions on the surfaces of the carbon materials. The pore structure and pore size distribution of the carbon material was characterized by N_2 adsorption/desorption tests (Tristar II 3020, Mike Instruments, USA). The

N_2 adsorption amount under different relative pressures P/P_0 was measured at 77 K and determined by the BET method, where the specific surface, S_{BET}, was calculated using the BET method. The BJH method was used to fit the isotherm for the nitrogen adsorption/desorption and the pore diameter distribution curve.

2.3 Electrochemical performance test

The preparation of the working electrode was carried out as follows: First, 4 mg of hollow fiber filter membrane-based porous carbon material was weighed out and mixed uniformly with acetylene black and polytetrafluoroethylene at a mass ratio of 8: 1.5: 0.5. Then, this mixture was made into a slurry with absolute ethanol, uniformly spread out onto a 1 cm × 1 cm nickel foam, and then vacuum dried at 80 °C for 24 h. Next, the nickel foam was pressed by the tablet press for 1.5 min at 15 MPa to prepare the electrode.

For the electrochemical performance testing process, test was carried out using a three-electrode system consisting of hollow fiber filter membrane-based porous carbon material as the working electrode, a 1.5 cm^2 platinum plate electrode as the counter electrode, and a calomel electrode as the reference electrode. The electrolyte was 6 M KOH solution. Cyclic voltammetry is a test method that can be used to characterize the reaction on an electrode surface and enable discussion for the mechanism of the electrode reaction. The voltage was set in the range of − 1 V and 0 V and the scanning rate was varied from 5 mV s^{-1} to 200 mV s^{-1}. The specific capacitance C (F g^{-1}) was calculated based on the following formula:

$$C = \frac{\int IdV}{2 \cdot vm\Delta V} \tag{1}$$

where I (A cm^{-2}) is the current density, ΔV (V) is the voltage window, m (g) represents the weight of the active materials in the working electrode, and v (mV s^{-1}) refers to the scanning rate.

The current charging and discharging test is a test method that is used to investigate the potential change with time under constant current, study the performance of electrodes and capacitors, and calculate the specific capacitance. The constant current charge–discharge was tested under a voltage range of − 1 to 0 V and a charge–discharge current range of 0.5 mA to 20 mA. The specific capacitance C (F g^{-1}) can be expressed by the following formula:

$$C = \frac{I \cdot \Delta t}{m \cdot \Delta V} \tag{2}$$

where I (A) is the charge and discharge current, ΔV (V) is the voltage change during the discharge time, Δt (s) is the discharge time, and m (g) is the mass of the porous carbon material on the working electrode.

AC impedance is a test method that involves disturbing capacitors with a small amplitude AC signals followed by observation of the system's reaction to such disturbances from the steady state. It can also be used to measure the AC impedance of electrodes, which can then enable calculation of the electrochemical parameters of the electrodes. The AC impedance was measured in the frequency range of 0.01 Hz to 100 kHz with an AC amplitude of 5 mV.

3 Results and discussion

Figure 1 shows the XRD spectrum for the porous carbon material ZKC-T obtained at different carbonization temperatures. It can be seen from the figure that there are two distinct diffraction peaks in the 2θ diffraction angle range of 10° to 90°, which are located at 21.8° and 43.4°, respectively. This corresponds to the (002) crystal plane and (101) crystal plane of graphite. Compared with standard graphite $2\theta \approx 26.6°$, the (002) diffraction peak for the porous carbon material ZKC-T is located at 21.8°. Therefore, a significant shift phenomenon (moving to a low diffraction angle) is observed. According to the Bragg formula ($2d \bullet \sin\theta = \lambda$), this phenomenon occurs because the interlayer spacing of the (002) crystal plane is increased [18, 19]. This is mainly because during the chemical activation process of pyrolysis at high temperature, the generated K atoms enter the graphite microcrystalline graphite layers, resulting in an increase in the interlayer spacing. Thus, the porous carbon material ZKC-T is confirmed to have an amorphous structure. At the same time, a low intensity diffraction peak is observed at 43.3°, indicating that a carbon nanosheet structure is contained within the porous carbon material ZKC-T [20].

To further investigate the structure and degree of disorder for the porous carbon material ZKC-T, the porous carbon material ZKC-T was characterized by Raman spectroscopy.

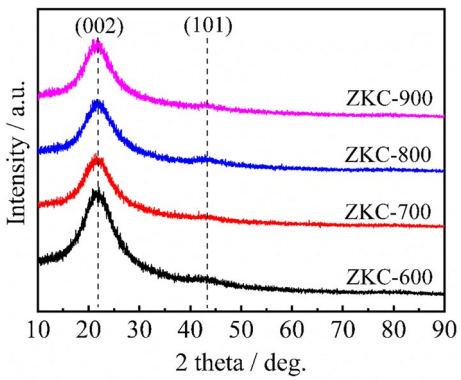

Fig. 1 X-ray diffraction spectra for ZKC-T

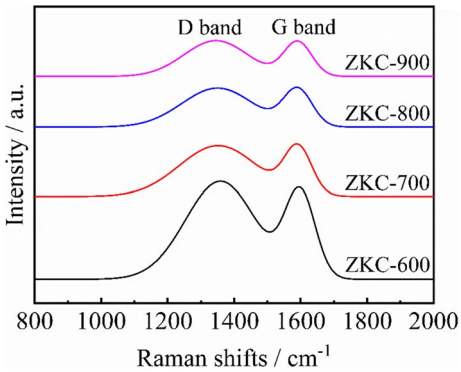

Fig. 2 Raman spectroscopy of ZKC-T

Figure 2 shows the Raman spectrum for the porous carbon material ZKC-T (600/700/800/900). In the wavenumber interval of 1000 ~ 1800 cm^{-1}, it can be seen that the Raman curve for the porous carbon material ZKC-T contains two typical peaks. They correspond to the D band at approximately 1347 cm^{-1} and the G band at approximately 1589 cm^{-1}, respectively. The D band reflects the disorder in the disordered carbon or lattice structure, while the G band reflects the in-plane stretching vibration of the sp^2 hybrid carbon atom E_{2g} phonon [21]. The I_D/I_G value is commonly used to calculate the intensity relationship for the two peaks. The larger the I_D/I_G value, the higher the degree of structural disorder of the carbon material and the lower the degree of graphitization [22]. The I_D/I_G values for the hollow fiber membrane-based porous carbon ZKC-600, ZKC-700, ZKC-800, and ZKC-900 were determined to be 1.427, 1.416, 1.411, and 1.371, respectively. As the carbonization temperature increases, the I_D/I_G value decreases, indicating that the graphite layer defects in the carbon material are gradually reduced and that the degree of graphitization is gradually increased.

To observe the internal micro-channel structure and size of the porous carbon material ZKC-T, TEM techniques were used for characterization and analysis. Figure 3a, b shows transmission electron micrographs of the porous carbon material ZKC-700 at different high magnifications. It can be observed that the carbon material ZKC-700 shows good light permeability. The dense and rich light points indicate that the material has a dense pore structure. Figure 3b shows a partially enlarged image of Fig. 3a. It can be seen that the carbon material ZKC-700 has a very high degree of disorder, indicating that the carbon material ZKC-700 has an amorphous structure. This is due to the etching effect of KOH on the carbon material during the high-temperature pyrolysis activation process, which results in an increase in lattice defects and the formation of a rich and disordered pore structure.

The N_2 adsorption/desorption curve for ZKC-T is shown in Fig. 4a, it can be seen that the N_2 adsorption/desorption curve for ZKC-T conforms to the I + IV type isothermal temperature line defined by the International Union of Pure

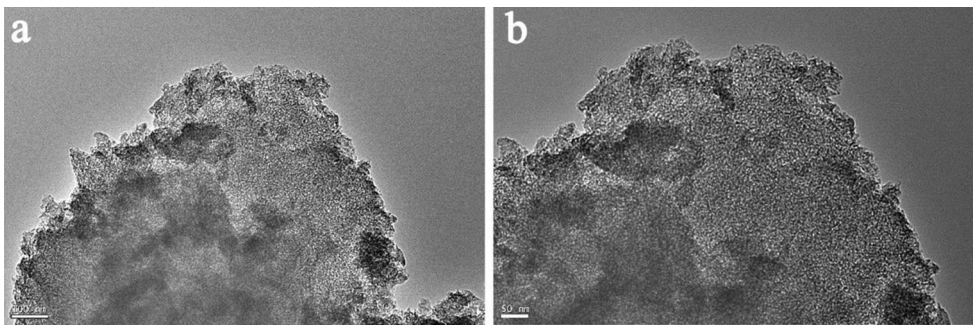

Fig. 3 TEM (**a**, **b**) of hollow fiber filter membrane-based porous carbon ZKC-700 (ruler: **a** 100 nm, **b** 50 nm)

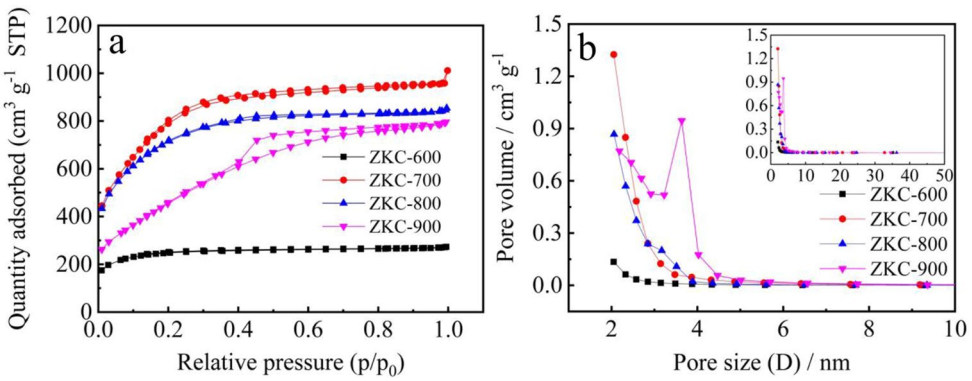

Fig. 4 N_2 adsorption/desorption curve of ZKC-T (**a**); pore size distribution curve of ZKC-T (**b**)

and Applied Chemistry (IUPAC). This indicates that the material is rich in micro-mesopores [23, 24]. For a relative pressure below 0.01, the adsorption of N_2 is mainly carried out by micropores, and the adsorption amount increases significantly, which means that the ZKC-T material consists of a rich micropore structure. For a relative pressure close to 0.4, a more obvious "hysteresis loop" appears, indicating that there is a certain mesoporous structure in the material. The curve for the ZKC-900 material shows a more typical "hysteresis loop", which is much larger than the "hysteresis loop" found in the ZKC-600, ZKC-700, and ZKC-800 materials, indicating that there are relatively many more mesoporous structures in the BZTC-900. In the stage where the relative pressure (P/P_0) changes from the low-pressure region to the high-pressure region, the XDC-T curve shows a typical steady upward trend. This is due to the increase in P/P_0, which forces N_2 into the interior of the porous carbon layer/multilayer N_2 adsorption. For a relative pressure close to 1.0, the N_2 adsorption capacity of ZKC-700 increases significantly, indicating that there are large pores in the hollow fiber membrane-based porous carbon ZKC-T. Figure 4b shows the pore size distribution diagram for ZKC-T. It can be seen that the material contains a large number of micro-mesopores, which are mainly concentrated near 2 nm in size; this is mainly due to the activation of KOH during the pyrolysis activation process at high temperature. At the same time, ZKC -900 also shows a peak approximately 3.6 nm, which indicates that a large number of mesoporous structures exist in the material ZKC-900. As shown in Table 1, the average pore size in ZKC-T (600/700/800/900) is 1.95 nm, 2.01 nm, 2.01 nm, and 2.86 nm, because the ionic radius in the electrolyte is less than 0.4 nm. Therefore, this type of pore size enables the electrolyte ions to access an efficient transmission channel and is beneficial to the generation of electric double layer capacitance [25]. The specific surface area of ZKC-T (600/700/800/900) was determined to be 856 $m^2\ g^{-1}$, 2934 $m^2\ g^{-1}$, 2582 $m^2\ g^{-1}$, 1701 $m^2\ g^{-1}$, respectively. The specific surface area for ZKC-600, ZKC-700, ZKC-800 and ZKC-900 shows the trend of an initial increase followed by a decrease. This is because high temperature plays a positive role in the activation of KOH during the high-temperature pyrolysis activation process, which helps to increase the specific surface area. However, as the temperature continues to increase, the increased pore size will lead to a collapse of the internal pores in the carbon material, resulting in a decrease in specific surface area.

Table 1 Summary of BET information for ZKC-T

Samples	S_{BET} ($m^2\ g^{-1}$)	Total pore volume ($cm^3\ g^{-1}$)	Average pore sizes (nm)
ZKC-600	856	0.42	1.95
ZKC-700	2934	1.48	2.01
ZKC-800	2482	1.30	2.01
ZKC-900	1701	1.21	2.86

X-ray photoelectron spectroscopy (XPS) was used to analyse the surface elements, content and surface functional groups for the porous carbon material ZKC-700. The full XPS spectrum for ZKC-700 is shown in Fig. 5a, with three characteristic peaks observed, corresponding to C1s, N1s, and O1s, respectively. The C, N and O content accounted for 88.29%, 3.73% and 7.98% of the total content, respectively. Numerous studies have shown that nitrogen and oxygen functional groups can participate in redox reactions to form pseudo capacitors. Nitrogen and oxygen functional groups can improve the wettability and electrical conductivity of a material and facilitate the formation of an electric double layer [26, 27]. The C1s spectrum of the porous carbon material ZKC-700 is shown in Fig. 5b, and three peaks can be fitted to the data. The strongest peaks are found to be located at 284.5 eV and 285.1 eV, corresponding to C = C and C–C/C-N [28–30], respectively; the peaks located at 286.4 eV correspond to C-O [31, 32]. Figure 5c shows the N1s spectrum for ZKC-700, which can be fitted to four main peaks. The peaks at 398.4 eV, 399.8 eV, 400.7 eV, and 402.1 eV correspond to N-6 (pyridinic-N), N-5 (pyrrolic-N), NQ (quaternary-N), and N-x (pyridine-N-oxide) [33–35], respectively. Figure 5d shows the O1s spectrum for ZKC-700, which can be fit to three characteristic peaks. The peaks at 531.4 eV, 532.5 eV, and 533.6 eV correspond to C = O (ester), C = O (carboxyl), and O-C = O, respectively [36, 37].

Figure 6a shows the CV curve obtained for hollow fiber filter-based porous carbon ZKC-T prepared at different carbonization temperatures in a 6 M KOH electrolyte at a scan rate of 10 mV s^{-1}. It can be seen from Fig. 6a that there is a certain redox bump in the CV curve for the porous carbon material ZKC-T. This is due to the nitrogen and oxygen functional groups present in the ZKC-T [38]. The CV curve for ZKC-700 was calculated, and its graphic integral area was found to be the largest; so, the porous carbon material ZKC-700 shows the best specific capacitance. Figure 6b shows the GCD curve measured for the porous carbon material ZKC-T in a 6 M KOH electrolyte with a current density of 1 A g^{-1}. It can be seen from the figure that, except for the material ZKC-600, all the other samples show an "isosceles triangle" shape, indicating good symmetry. A small part of the curve deviates from the linear relationship, which corresponds to the redox uplift in Fig. 6a. According to the GCD curve calculation, the specific capacitances for the porous carbon materials ZKC-600, ZKC-700, ZKC-800, and ZKC-900 are 262 F g^{-1}, 289 F g^{-1}, 230 F g^{-1} and 204 F g^{-1}, respectively, at a current density of 1 A g^{-1}. It can be seen that the specific capacitance of the porous carbon material ZKC-700 is larger, which is the same as the result

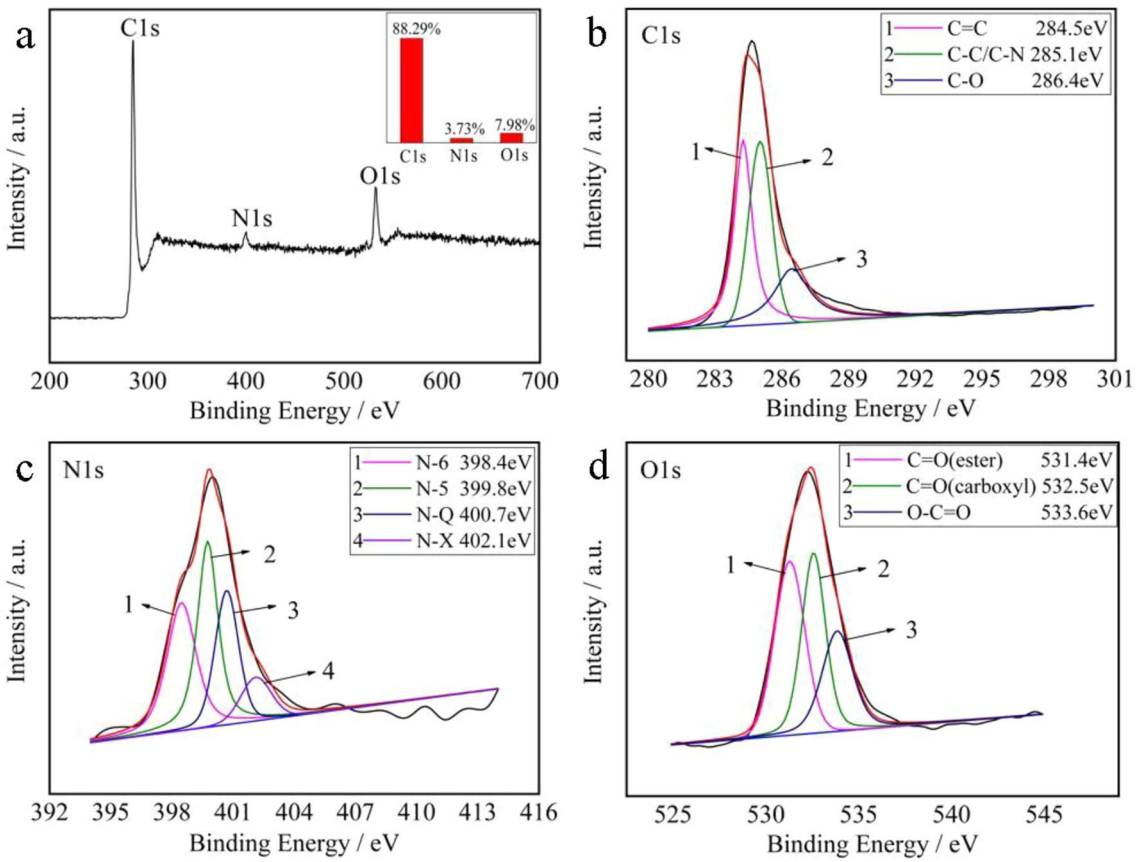

Fig. 5 Elemental composition XPS spectrum for hollow fiber filter membrane-based porous carbon ZKC-700: full Spectrum (**a**), C1s (**b**), N1s (**c**), and O1s (**d**)

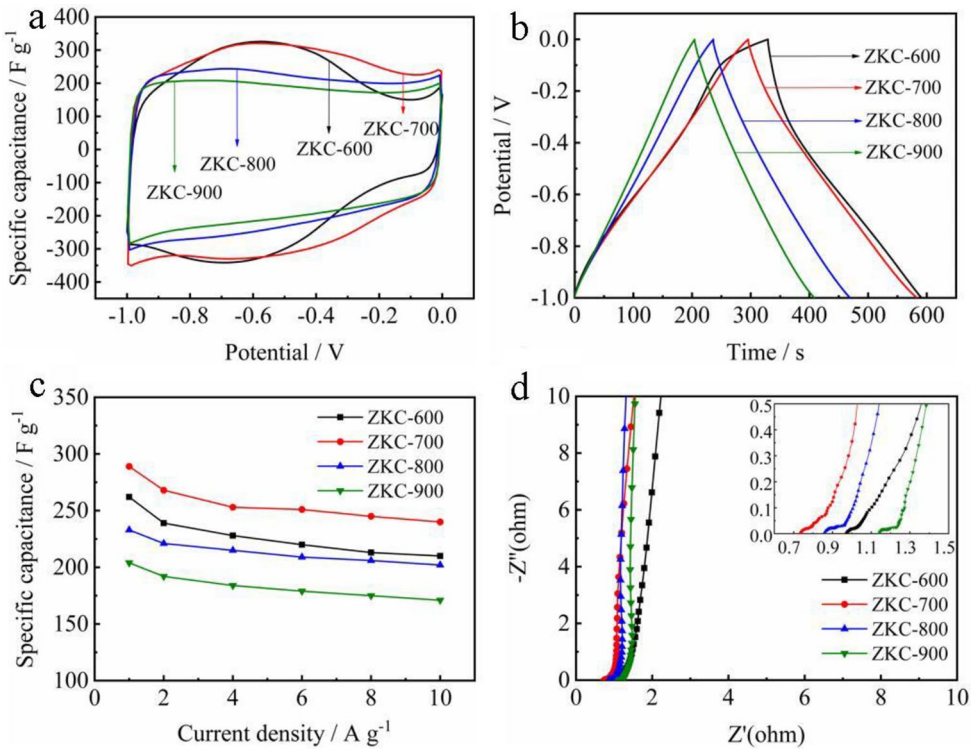

Fig. 6 Electrochemical performance tests for ZKC-T: CV curve with scan rate of 10 mV s^{-1} (**a**); GCD curve with current density of 1 A g^{-1} (**b**); specific capacitance based on the GCD curve (**c**); and the Nernst diagram (**d**)

obtained from the CV curve shown in Fig. 6a. Figure 6c shows the specific capacitance calculated at different current densities at different carbonization temperatures and calculated according to the GCD curve. It can be seen from this comparison that the capacitance performance of the porous carbon material ZKC-700 is significantly higher than that of the other carbon materials prepared at different temperatures, which is mainly due to a high specific surface area of 2934 $m^2\ g^{-1}$, abundant nitrogen and oxygen, and reasonable pore size structure. This helps the electrolyte to be immersed into the carbon material more smoothly, which is beneficial to the rapid transfer of electrolyte ions; thus, the specific surface area of the carbon material is used efficiently, which results in an improvement in the electrochemical performance of the material. As the current density is increased from 1 A g^{-1} to 10 A g^{-1}, the specific capacitance for ZKC-700 decays from 289 F g^{-1} to 240 F g^{-1}, and the specific capacitance attenuation rate of this material is determined to be 17%. This proves that the porous carbon material ZKC-700 has a good rate performance. The Nernst diagram for ZKC-T is shown in Fig. 6d. In the low frequency region, except for ZKC-600, the curves for ZKC-700, ZKC-800, and ZKC-900 are nearly perpendicular to the horizontal axis, indicating that the porous carbon material ZKC-T shows excellent capacitor behaviour. At the same time, in the high frequency region, the AC series resistance (AC-ESR) for the porous carbon materials ZKC-600, ZKC-700, ZKC-800, and ZKC-900 was determined to be 0.97 Ω, 0.73 Ω, 0.86 Ω, and 1.14 Ω, respectively. The half-ring structure in the high-frequency region is due to the existence of a pseudo charge transfer resistance. The smaller half-circle indicates faster charge transfer [39].

Figure 7a shows the CV curve measured for the porous carbon material ZKC-700 at different scan rates. It can be observed that the CV curves obtained for the porous carbon ZKC-700 at different scan rates all show a rectangular-like outline. The CV curves measured for materials at different scan rates exhibit good capacitance performance. Figure 7b shows the GCD curve obtained for porous carbon ZKC-700 at different current densities. It is not difficult to see that the GCD curves under different current densities maintain the shape of an isosceles triangle, indicating that the porous carbon ZKC-700 has excellent capacitance performance and electrochemical reversibility [40]. Figure 7 (c) shows the results from a cycle life test. At a current density of 1 A g^{-1}, after 5000 charge and discharge cycles, the ZKC-700 has a capacitance retention rate of 92.8%, and the material exhibits excellent stability.

The effect of activator concentration on the capacitance performance of ZKC-700 during activation was further investigated. Figure 8a shows the CV curve measured for hollow fiber filter-based porous carbon ZKC-700-H at a scan rate of 10 mV s^{-1}. It can be seen from Fig. 8a that there is a certain redox bump in the CV curve for the porous carbon material ZKC-T, which is mainly attributed to the nitrogen and oxygen surface functional groups present in the porous carbon material ZKC-T. The CV curve for ZKC-700–1:4

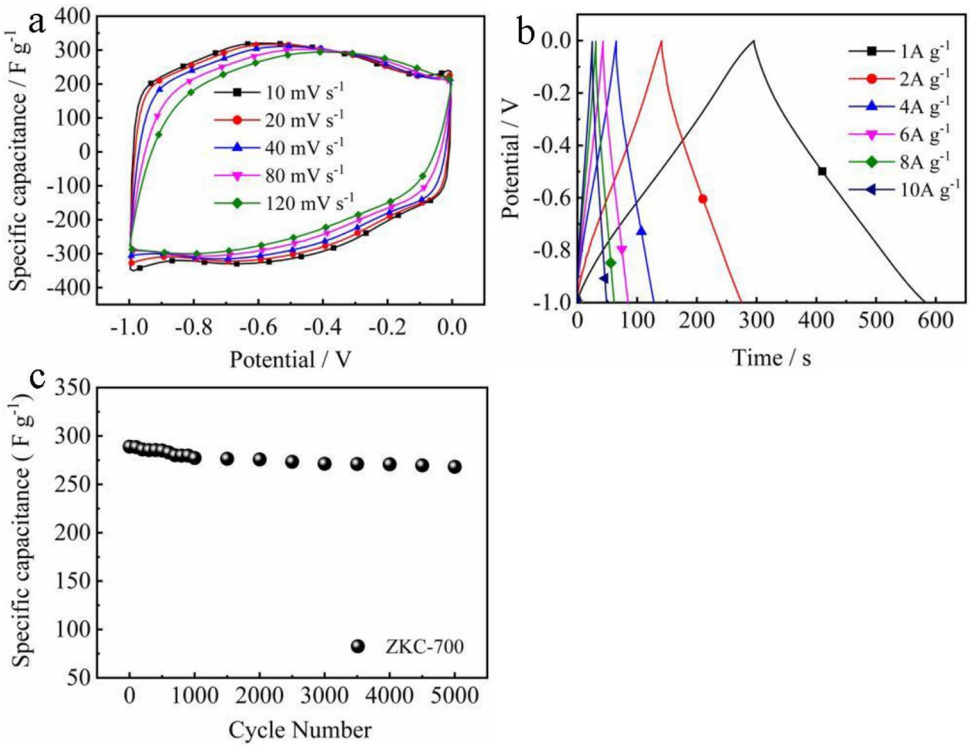

Fig. 7 Electrochemical performance tests for ZKC-700: CV curve at different scan rates (**a**); GCD curve at different current densities (**b**); cycle life test (**c**)

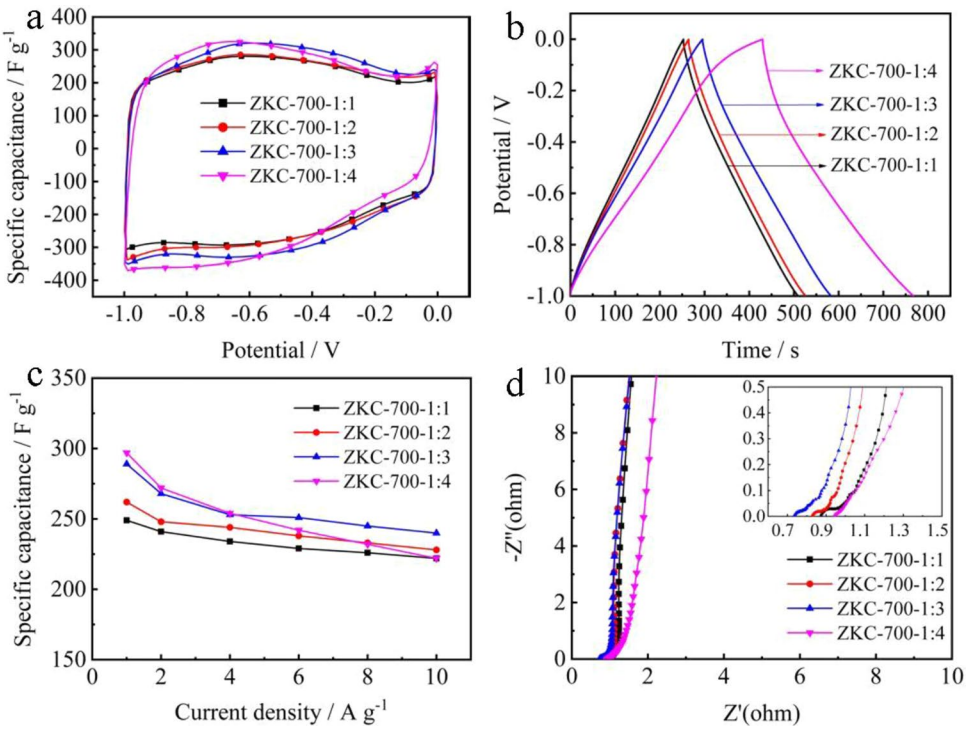

Fig. 8 Electrochemical performance of ZKC-700-H: CV curve with scan rate of 10 mV s^{-1} (**a**); GCD curve with current density of 1 A g^{-1} (**b**); specific capacitance based on the GCD curve (**c**); and the Nernst diagram (**d**)

was calculated and its graphic integral area was determined to be the largest; so, ZKC-700–1:4 shows the largest specific capacitance value. Figure 8b shows the GCD curve for the porous carbon material ZKC-700-H in a 6 M KOH electrolyte at a current density of 1 A g^{-1}. It can be seen from the figure that except for the material ZKC-700–1:4, the rest of the samples show an "isosceles triangle" shape, indicating good symmetry, which shows that the porous carbon material ZKC-700-H has excellent electrochemical reversibility. According to the GCD curve calculation, at a current density of 1 A g^{-1}, the specific capacitances of the porous carbon materials ZKC-700–1:1, ZKC-700–1:2, ZKC-700–1:3, ZKC-700–1:4 are 249 F g^{-1}, 268 F g^{-1}, 289 F g^{-1}, and 297 F g^{-1}, respectively, which shows that the specific capacitance of ZKC-700–1:4 is larger. This shows that the CV curve results in Fig. 8a are the same. Figure 8c shows the trend graph for the change in specific capacitance at different current densities calculated from the GCD curve. After comparison, the specific capacitance value of the carbon material ZKC-700–1:4 was found to be the largest, but as the current density increases, the specific capacitance value of the ZKC-700–1:4 attenuates more, and even appears to be lower than that for ZKC-700–1:3. This is largely due to the shortened charge and discharge time at high current densities, resulting in electrolyte ions not having enough time to enter the internal pores of the carbon material, and the contribution of pseudo capacitance to capacitance. The Nernst diagram for ZKC-700-H is shown in Fig. 8d. In the low frequency region, the curves for ZKC-700–1:2, ZKC-700–1:3, and ZKC-700–1:4 are found to be almost perpendicular to the horizontal axis, with only the curve for ZKC-700–1:4 showing a slight inclination, indicating that the porous carbon material ZKC-700-H shows excellent capacitor behaviour. At the same time, in the high frequency region, the AC series resistance (AC-ESR) for the porous carbon materials ZKC-700–1:1, ZKC-700–1:2, ZKC-700–1:3, ZKC-700–1:4 was determined to be 0.87 Ω, 0.82 Ω, 0.73 Ω, and 0.95 Ω, respectively. It can be seen that the porous carbon material ZKC-700–1:3 shows the smallest AC series resistance value and a very small pseudo charge transfer resistance.

4 Conclusion

In this paper, a waste hollow fiber filter membrane was used as a carbon source to prepare a hollow fiber filter-based porous carbon material ZKC-T by pre-carbonization-KOH activation. With the help of a series of characterization methods, the porous carbon material ZKC-T was determined to be composed of amorphous carbon. The porous carbon material ZKC-700 shows a specific surface area of up to 2934 m^2 g^{-1}. The porous carbon ZKC-T is mainly composed of a micro-mesoporous structure, which contributes to efficient transport of electrolyte ions and improved electrochemical performance. The material exhibits excellent electrochemical performance. In a 6 M KOH electrolyte, the specific capacitance for ZKC-700 was found to be as high as 289 F g^{-1} at a current density of 1 A g^{-1}. This material shows a

good rate performance. As the current density was increased from 1 A g^{-1} to 10 A g^{-1}, the specific capacitance decreased from 289 F g^{-1} to 240 F g^{-1}, with an attenuation rate of only 17%. After 5000 cycles of constant current charge and discharge, the specific capacitance retention rate for ZKC-700 was found to be 92.8%, indicating excellent stability. We believe that the application of solid waste polymer materials in the preparation of high-performance electrode carbon materials has certain potential value and can help alleviate the white pollution problem.

Acknowledgements This effort was supported by the National Natural Science Foundation of China (21364004 and 21664009), Gansu Province University Fundamental Research Funds and the Doctor Research Fund of Lanzhou University of Technology, P.R. China.

References

1. Hu D, Chen CY, Liu Q (2018) Fabrication of hollow carbon spheres with robust and significantly enhanced capacitance behaviors. J Mater Sci 53:12310–12321
2. Sankar KV, Seo Y, Lee SC, Jun SC (2018) Redox additive-improved electrochemically and structurally robust binder-free nickel pyrophosphate nanorods as superior cathode for hybrid supercapacitors. ACS Appl Mater Interfaces 10:8045–8056
3. Piao JY, Bin DS, Duan SY, Lin XJ, Zhang D, Cao AM (2018) A facile template free synthesis of porous carbon nanospheres with high capacitive performance. Sci China Chem 61:538–544
4. Yu M, Ma YX, Liu JH, Li SM (2015) Polyaniline nanocone arrays synthesized on three-dimensional graphene network by electrodeposition for supercapacitor electrodes. Carbon 87:98–105
5. Haladkar SA, Desai MA, Sartale SD, Alegaonkar PS (2018) Assessment of ecologically prepared carbon-nano-spheres for fabrication of flexible and durable supercell devices. J Mater Chem A 6:7246–7256
6. Kim C, Ngoc BT, Yang KS et al (2007) Self-sustained thin webs consisting of porous carbon nanofibers for supercapacitors via the electrospinning of polyacrylonitrile solutions containing zinc chloride. Adv Mater 19:2341–2346
7. Du W, Bai YL, Xu JQ et al (2018) Advanced metal-organic frameworks (MOFs) and their derived electrode materials for supercapacitors. J Power Sources 402:281–295
8. Lu WJ, Liu MX, Miao L et al (2016) Nitrogen-containing ultramicroporous carbon nanospheres for high performance supercapacitor electrodes. Electrochim Acta 205:132–141
9. Chen C, Yu DF, Zhao GY et al (2016) Three-dimensional scaffolding framework of porous carbon nanosheets derived from plant wastes for high-performance supercapacitors. Nano Energy 27:377–389
10. Chen AB, Li YQ, Liu L et al (2017) Controllable synthesis of nitrogen-doped hollow mesoporous carbon spheres using ionic liquids as template for supercapacitors. Appl Surf Sci 393:151–158
11. Kim BS, Lee K, Kang S et al (2017) 2D reentrant auxetic structures of graphene/CNT networks for omnidirectionally stretchable supercapacitors. Nanoscale 9:13272–13280
12. Tonurist K, Janes A, Thomberg T, Kurig H, Lust E (2009) Influence of mesoporous separator properties on the parameters of electrical double-layer capacitor single cells. J Electrochem Soc 156:A334–A342
13. Shang YY, Yu Z, Xie C et al (2015) A facile fabrication of MnO2/graphene hybrid microspheres with a porous secondary structure for high performance supercapacitors. J Solid State Electrochem 19:949–956
14. Zhong C, Deng YD, Hu WB, Qiao JL, Zhang L, Zhang JJ (2015) A review of electrolyte materials and compositions for electrochemical supercapacitors. Chem Soc Rev 44:7484–7539
15. Plitz I, DuPasquier A, Badway F et al (2006) The design of alternative nonaqueous high power chemistries. Appl Phys A 82:615–626
16. Jiang WM, Jia XH, Luo ZJ, Wu XY (2014) Supercapacitor performance of spherical nanoporous carbon obtained by a CaCO3-assisted template carbonization method from polytetrafluoroethene waste and the electrochemical enhancement by the nitridation of CO(NH2)(2). Electrochim Acta 147:183–191
17. Zhang YX, Shen ZM, Yu YF, Liu L, Wang GX, Chen AB (2018) Porous carbon derived from waste polystyrene foam for supercapacitor. J Mater Sci 53:12115–12122
18. Wang Y, Su FB, Wood CD, Lee JY, Zhao XS (2008) Preparation and characterization of carbon nanospheres as anode materials in lithium-ion secondary batteries. Ind Eng Chem Res 47:2294–2300
19. Rajagopal RR, Aravinda LS, Rajarao R, Bhat BR, Sahajwalla V (2016) Activated carbon derived from non-metallic printed circuit board waste for supercapacitor application. Electrochim Acta 211:488–498
20. Luo HM, Yang YF, Chen YZ, Zhang JQ, Zhao X (2016) Structure and electrochemical performance of highly porous carbons by single-step potassium humate carbonization for application in supercapacitors. J Appl Electrochem 46:113–121
21. Zeng R, Tang XN, Huang BY, Yuan K, Chen YW (2018) Nitrogen-doped hierarchically porous carbon materials with enhanced performance for supercapacitor. ChemElectroChem 5:515–522
22. Tang ZJ, Pei ZX, Wang ZF et al (2018) Highly anisotropic, multichannel wood carbon with optimized heteroatom doping for supercapacitor and oxygen reduction reaction. Carbon 130:532–543
23. Lian YM, Ni M, Huang ZH et al (2019) Polyethylene waste carbons with a mesoporous network towards highly efficient supercapacitors. Chem Eng J 366:313–320
24. Gómez-Serrano V, González-Garcıa C, González-Martın M (2001) Nitrogen adsorption isotherms on carbonaceous materials. comparison of BET and Langmuir surface areas. Powder Technol 116:103–108
25. Zhai YP, Dou YQ, Zhao DY, Fulvio PF, Mayes RT, Dai S (2011) Carbon materials for chemical capacitive energy storage. Adv Mater 23:4828–4850
26. Zhang JJ, Fan HX, Dai XH, Yuan SJ (2018) Digested sludge-derived three-dimensional hierarchical porous carbon for high-performance supercapacitor electrode. R Soc Open Sci 5:172456
27. Luo L, Chen T, Li Z, Zhang Z, Zhao W, Fan M (2018) Heteroatom self-doped activated biocarbons from fir bark and their excellent performance for carbon dioxide adsorption. J Co2 Util 25:89–98
28. Kulkarni SB, Patil UM, Shackery I et al (2014) High-performance supercapacitor electrode based on a polyaniline nanofibers/3D graphene framework as an efficient charge transporter. J Mater Chem A 2:4989–4998
29. Liu XJ, Zhou YC, Zhou WJ, Li LG, Huang SB, Chen SW (2015) Biomass-derived nitrogen self-doped porous carbon as effective metal-free catalysts for oxygen reduction reaction. Nanoscale 7:6136–6142
30. Wang Q, Yan J, Wang YB et al (2014) Three-dimensional flower-like and hierarchical porous carbon materials as high-rate performance electrodes for supercapacitors. Carbon 67:119–127
31. Tan YM, Xu CF, Chen GX, Fang XL, Zheng NF, Xie QJ (2012) Facile synthesis of manganese-oxide-containing mesoporous nitrogen-doped carbon for efficient oxygen reduction. Adv Funct Mater 22:4584–4591

32. Reiche S, Blume R, Zhao XC et al (2014) Reactivity of mesoporous carbon against water–An in-situ XPS study. Carbon 77:175–183
33. Sanchez-Sanchez A, Suarez-Garcia F, Martinez-Alonso A, Tascon JMD (2014) Aromatic polyamides as new precursors of nitrogen and oxygen-doped ordered mesoporous carbons. Carbon 70:119–129
34. Zhang DY, Han M, Li YB et al (2017) Ultra-facile fabrication of phosphorus doped egg-like hierarchic porous carbon with superior supercapacitance performance by microwave irradiation combining with self-activation strategy. J Power Sources 372:260–269
35. Kundu S, Xia W, Busser W et al (2010) The formation of nitrogen-containing functional groups on carbon nanotube surfaces: a quantitative XPS and TPD study. Phys Chem Chem Phys 12:4351–4359
36. Patel MA, Luo FX, Savaram K et al (2017) P and S dual-doped graphitic porous carbon for aerobic oxidation reactions: Enhanced catalytic activity and catalytic sites. Carbon 114:383–392
37. Wen YY, Wang B, Huang CC, Wang LZ, Hulicova-Jurcakova D (2015) Synthesis of phosphorus-doped graphene and its wide potential window in aqueous supercapacitors. Chem-Eur J 21:80–85
38. Zhang JQ, Song SY, Xue JC et al (2018) Nitrogen-rich Porous carbon derived from biomass as high performance electrode materials for supercapacitors. Int J Electrochem Sci 13:5204–5218
39. Yang CS, Jang YS, Jeong HK (2014) Bamboo-based activated carbon for supercapacitor applications. Curr Appl Phys 14:1616–1620
40. Guan BY, Kushima A, Yu L, Li S, Li J, Lou XW (2017) Coordination polymers derived general synthesis of multishelled mixed metal-oxide particles for hybrid supercapacitors. Adv Mater 29:1–8

Authors and Affiliations

He Zhu[1] · Zhishang Gao[1] · Songhong Fan[1] · Mingjian Zhang[1] · Zhangzhang Tang[1] · Zhong Ren[1] · Huixia Feng[1] · Heming Luo[1] · Jianqiang Zhang[1]

✉ Heming Luo
luohm666@163.com

✉ Jianqiang Zhang
zhangjq@lut.edu.cn

[1] School of Petrochemical Engineering, Lan Zhou University of Technology, Lanzhou 730050, China